Journal of Power Sources 480 (2020) 229147

Contents lists available at ScienceDirect

Journal of Power Sources

journal homepage: www.elsevier.com/locate/jpowsour

A two-stage sodium thermal electrochemical converter: Parametric optimization and performance enhancement

Wanli Peng [a,b], Julian Gonzalez-Ayala [b,c], Shanhe Su [a], Jincan Chen [a,*], Antonio Calvo Hernández [b,c,**]

[a] Department of Physics, Xiamen University, Xiamen, 361005, People's Republic of China
[b] Departamento de Física Aplicada, Universidad de Salamanca, 37008, Salamanca, Spain
[c] Instituto de Física Fundamental y Matemáticas, Universidad de Salamanca, 37008, Salamanca, Spain

HIGHLIGHTS

- A two-stage sodium thermal electrochemical converter is updated.
- Main irreversible losses are considered and the coupling of two stages is optimized.
- The maximum efficiency and power output density increase 17.5% and 40.6%.
- The optimum selection criteria of main parameters are supplied.
- The optimum energetic space is given by the Pareto front.

ARTICLE INFO

Keywords:
Two-stage sodium thermal electrochemical converter
Main irreversible loss
Optimum operation state
Pareto front
Parametric selection criterion

ABSTRACT

An asymmetric two-stage sodium thermal electrochemical converter and its optimum performance are studied by means of an improved analytical model including the main losses in the overall system. Based on the study of a single-stage sodium thermal electrochemical converter, the inner process is divided into two stages including one at the 1300 K temperature (evaporator) and the other at the 800–1300 K intermediate temperature with the aim of improving efficiency. The parametric optimum selection criteria of a few main parameters of the two-stage device are provided and the coupling of the separate stages in an overall optimum system in terms of the appropriate intermediate temperature is particularly stressed. The maximum efficiency of the proposed overall system can attain 36.2%, which is 17.5% higher than that of the best performing single-stage device, and increase up to 34.1% and 24.8% over the existing two-stage devices designed by two research groups, respectively. The Pareto front obtained from numerical multiobjective and multiparametric methods endorses previous findings and visually presents the space of the states and the energetic properties of the overall arrangement compared with the corresponding data for the isolated first and second stages.

1. Introduction

A sodium thermal electrochemical converter (Na-TEC), which is one promising thermally regenerative electrochemical system, converts directly heat into electricity by the isothermal expansion of sodium ions through a β''-alumina solid-electrolyte (BASE) allowing for Na^+ ion transport in a wide temperature range [1,2]. The emerging Na-TEC [also named as the alkali metal thermal electric converter (AMTEC)] can be traced back to the 1960s, and the technology, primarily for the NASA Pluto/Express spacecraft mission [3], attracted extensive attention in the 1990–2000s for space applications. Some seminal studies on Na-TEC systems have been reported. For example, Weber [4] presented a theoretical analysis and described the construction of a model beta-alumina thermoelectric generator. Cole [2] studied the thermodynamic operating principles and gave some crucial expressions including current-voltage relation and efficiency. Williams et al. investigated the kinetics and transport at electrodes including the interfacial impedance model [5] and the dependence of the interfacial impedance of Na (g)/porous Mo/Na-Beta-double prime alumina on temperature [6]. It is

* Corresponding author.
** Corresponding author. Departamento de Física Aplicada, Universidad de Salamanca, 37008 Salamanca, Spain.
E-mail addresses: jcchen@xmu.edu.cn (J. Chen), anca@usal.es (A.C. Hernández).

https://doi.org/10.1016/j.jpowsour.2020.229147
Received 14 August 2020; Received in revised form 7 October 2020; Accepted 28 October 2020
0378-7753/

Nomenclature

A	electrode area on BASE tube, m^2
B	charge-exchange coefficient, A $K^{1/2}$/(Pa m^2)
c_P	average molar specific heat, J/(mol K)
D	BASE thickness, m
F	Faraday constant, C/mol
G	pressure loss geometric factor
J	current density of single, A/m^2
L	latent heat, J/g
M	molecular weight, g/mol
P	power output, W
p	POD, W/m^2
p_{sat}	saturation vapor pressure, P_a
R	gas constant, J/(mol K)
T_C	condenser temperature, K
T_H	evaporator temperature, K
T_{in}	intermediate temperature, K
T_0	environment temperature, K
V_{ac}	over potential difference, V
V_R	ionic BASE voltage, V
Z	geometric factor

Greek symbols

η	efficiency
μ	a coefficient, m^2
σ	Stefan-Boltzmann constant, W/(m^2 K^4)

Subscripts

i (i = 1, 2) the i th stage max maximum

Abbreviations

AMTEC	alkali metal thermoelectric converter
BASE	β''-alumina solid electrolyte
MEF	maximum efficiency
MPO	maximum power output
MPOD	maximum power output density
Na-TEC	sodium thermal electrochemical converter
POD	power output density
TEG	thermoelectric generator

well known [7] that the efficiency of the most advanced heat engines can reach about 40% currently. Heat is directly converted to work in the isothermal ion expansion process in the Na-TEC, which can be modelled as a heat engine. In comparison, the ideal efficiency of the Na-TEC can be achieved approximately 92–95% of the efficiency of the Carnot heat engine operating the temperatures between 450 and 1300 K [8]. However, the practical efficiency of Na-TECs can only reach 20% for the systems at the high-temperature region of 1050–1150 K and low-temperature region of 550–625 K [9].

Some key technical challenges such as the degradation of the constituent materials [10], the high temperature sealing, and the electrolyte stability [11], has resulted in actual efficiency falling far short of the ideal efficiency. Many researchers carried out experimental and theoretical investigations to improve the efficiency and power output with significant results. For example, Nakata et al. [12] prepared TiN, TiC, TiC/TiN, and Mo electrodes for a Na-TEC by ceramic processing and studied their cathodic polarization characteristics at 600–800 °C. Lodhi et al. [13] improved the efficiency of Na-TEC to 17.5% by changing some geometrical dimensions. Lodhi et al. [14] further dealt with the problem of power degradation in some detail and proposed some suggested measures to diminish loss of power with time. Lodhi et al. also investigated temperature dependent of grain growth model for Na-TEC electrodes [15] and BASE performance in an AMTEC [16]. El Genk et al. [17] identified a number of design changes to improve the performance of PX-series cells, such as increasing the BASE tube number and the BASE electrode length, developing corrugated BASE tubes, and using highly thermally conductive refractory metals (Ni or Mo) on the cell hot side. Peng et al. [18] discussed the dependence of the performance of the AMTEC on the BASE thickness and obtained the maximum efficiency (MEF) and maximum power output density (MPOD), which are, respectively, 22.3% and 6.83×10^3 W/m^2 at the evaporator temperature of 1170 K. Some coupled systems have been proposed to improve the whole system performance by utilizing the AMTEC exhaust heat. For example, Wu et al. [19] displayed the mathematical model of the AMTEC-thermoelectric generator (TEG) integrated system and obtained the efficiencies of 27.4% and 31.3% for the AMTEC and AMTEC/TEG, respectively. Peng et al. [20] further extended the AMTEC/TEG integrated system and found that MEF and MPOD could climb to 34.6% and 6.43×10^4 W/m^2 with an increment of 9.15% and 34.0% over that of the single AMTEC. Later on, a novel coupled system comprised of a Na-TEC and a Brayton heat engine was proposed by Peng et al. [21]. The MEF and MPOD of the system attain, respectively, 41.7% and 116×10^3 W/m^2, which increase 44.8% and 158% compared with that of the AMTEC working alone. In recent years, some researchers devoted themselves to improve the performance of a Na-TEC from a novel perspective by increasing the number of stages of the Na-TEC. For example, Balagopal et al. [22] provided a multi-stage sodium heat engine including at least two-stage and an electrical circuit operatively to convert thermal energy to electrical energy. Limia et al. [9] demonstrated the first time that a two-stage Na-TEC can increase the efficiency of 8% over the best performing single-stage device, and they further presented a thermal design of an asymmetric two-stage Na-TEC and achieved a 29% MEF and a 125 W maximum power output (MPO) [23].

Herein, we further demonstrate that the two-stage Na-TEC viewed as a series of engines [24,25] is more efficiently than already existed most efficient single Na-TEC and the former can improve the MEF and POD by up to 17.5% and 40.6% over the latter. Moreover, the MEF of the two-stage Na-TEC can improve 34.1% and 24.8% than that of two-stage Na-TECs reported in Refs. [9,23], respectively. In particular, the goal of this paper is twofold: a) to improve the model of a two-stage Na-TEC, and b) to investigate the optimum performance on the basis of the key parameters in regards with design and main losses: the BASE thickness, the current density, and the intermediate temperature between the two stages. Goal a) mainly relies on of the assumption of two single AMTEC coupled according to constraints imposed by the continuity and energy conservation (i.e., without heat leaks to the environment) so that the second AMTEC device works with heat delivered by the first one. For both of them heat transfer by conduction and radiation, and pressure drops through the porous electrodes by appropriate geometrical factors are considered. The additional assumption of the intermediate temperature for both stages rests on the work by Limia et al. [9] to minimize losses from overpotential and Ohmic contributions. As it will explained below, such an intermediate temperature could play a significant role in the performance regimes of the individual and collective behaviours. Goal b) focus in the analysis of the influence of some key parameters (as the extreme temperatures, current densities, cross sectional areas, and thickness BASEs) on the selected figures of merit: the power output density and thermal efficiency of the overall device. Thus, special attention is paid on the role of the intermediate temperature as it is found that only in a quite narrow interval of values the figures of merit achieve their corresponding maxima values.

Goals a) and b) are, respectively, accomplished in sections 2 and 3, where the performance regimes of the MEF and MPOD are analysed in terms of the optimum ranges of several key parameters. Section 4

contains a closer analysis on the influence of the intermediate temperature. Section 5 collects the main results obtained and a comparison with previous ones. Section 6 is committed to give a complementary perspective on configurations leading to the useful information of the optimal functions and parameters using a multiobjective and multiparametric optimization which is built on the Pareto front. Finally, Section 7 is devoted to conclusions and some perspectives of future works.

2. The description of a two-stage Na-TEC

The basic thermodynamic operating principles for a single Na-TEC were introduced [18]. The operating principles of a two-stage Na-TEC are similar to those of a single Na-TEC and its schematic diagram is shown in Fig. 1. q_H is the heat flow from the heat source to the evaporator plenum of the first stage Na-TEC at temperature T_H. q_C is the heat flow from the condenser plenum of the second stage Na-TEC at temperature T_C to the environment at temperature T_0. T_{in} is the temperature of the intermediate temperature plenum. $A_{1,2}$ corresponds to the first/second stage electrolyte area, $D_{1,2}$ is the first/second stage electrolyte thickness, and $P_{1,2}$ is the power output of the first/second stage Na-TEC, respectively. $P = P_1 + P_2$ is the total power output of the two-stage Na-TEC device.

In the first stage operation, liquid sodium is heated and vaporized in the high-temperature plenum. Sodium cations expand isothermally though the BASE from the high-temperature plenum into the intermediate plenum where the pressure is the vapor pressure at open circuit plus the pressure drop produced in the process of the recombination of electrons and ions and then flow through the porous electrode at the close circuit. The sodium vapor releases the heat q_{in} and cools at constant pressure, which is regenerated in full in the next stage Na-TEC. The sodium goes through the isothermal expansion process from the intermediate plenum to the low temperature condenser plenum in which the sodium cools and condenses to discharge the waste heat, q_C.

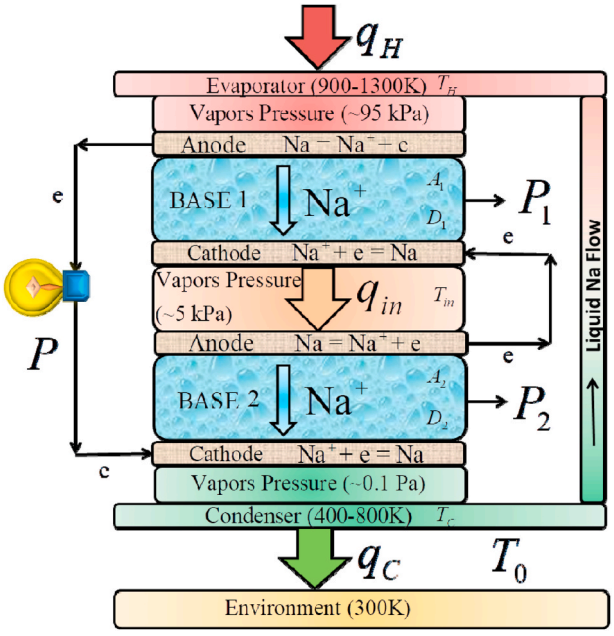

Fig. 1. The schematic diagram of a two-stage Na-TEC.

2.1. The efficiency of the first stage Na-TEC

The thermodynamic operation of the first stage Na-TEC is like that of a single Na-TEC. Thus, the first stage thermal first-law based efficiency, defined as the ratio of the total power output to total heat input, η_1 is given by [18]

$$\eta_1 = \frac{P_1}{q_H} = \frac{J_1 A_1 \left[\frac{RT_H}{F}\ln[1 + p_{sat}(T_H)\mu D_1/(RT_H)] - V_{ac,1} - V_{R,1}\right]}{J_1 A_1 \left[\frac{RT_H}{F}\ln[1 + p_{sat}(T_H)\mu D_1/(RT_H)] - V_{ac,1} - V_{R,1}\right] + J_1 A_1 ML \Big/ F + J_1 A_1 c_P (T_H - T_{in}) M \Big/ F + A_1 \sigma \left(T_H^4 - T_{in}{}^4\right) \Big/ z}, \quad (1)$$

where [14,26]

$V_{R,1} = J_1 D_1 [1.62 \times 10^{-5} T_H \exp(-45.5/T_H) + 1.55 \times 10^{-7} T_H \exp(3722/T_H)]$,

$$V_{ac,1} = -\frac{2RT_H}{F}\ln\left[\frac{1}{2}\left[\frac{J_1{}^2 T_H}{B_1{}^2 p_{sat}^2(T_H)} + 4\right]^{\frac{1}{2}} - \frac{1}{2}\frac{J_1\sqrt{T_H}}{B_1 p_{sat}(T_H)}\right] +$$

$$\frac{2RT_H}{F}\ln\left[\frac{1}{2}\left[\frac{J_1{}^2\sqrt{T_H T_{in}}}{B_1{}^2 p_{sat}(T_H) p_{sat}(T_{in})} + 4\left[1 + \frac{\left(1 + \frac{3G_1}{8\pi}\right)\sqrt{2\pi M R T_H T_{in}}\frac{J_1}{F}}{p_{sat}(T_{in})\sqrt{T_H}}\right]^{\frac{1}{2}}\right]\right.$$

$$\left. + \frac{1}{2}\frac{J_1 (T_H T_{in})^{\frac{1}{4}}}{B_1\sqrt{p_{sat}(T_H) p_{sat}(T_{in})}}\right],$$

$P_{sat}(T) = 10^{9.678 - 5383.2/T}$ is the saturation vapor pressure at temperature T[14], $V_{R,1}$ is the first stage ionic BASE voltage, $V_{ac,1}$ is the first stage over potential difference, G_1 is the first stage pressure loss geometric factor, B_1 denotes the first stage charge-exchange coefficient, J_1 the first stage current density, L and M are the sodium vaporization latent heat and molecular weight, c_P is the molar specific heat, z is the radiation reduction factor, F the Faraday constant, σ the Stefan-Boltzmann constant, μ is a coefficient, and R is the gas constant. The specific relational expression among T_H, μ, D_1, and T_{in} should satisfy the following relation [26]

$$\frac{p_{sat}(T_H)}{1 + p_{sat}(T_H)\mu D_1/(RT_H)} = p_{sat}(T_{in})\sqrt{\frac{T_H}{T_{in}}}. \quad (2)$$

2.2. The efficiency of the second stage Na-TEC

As shown in Fig. 1, the heat q_{in} from the first stage is fully utilized by the second stage Na-TEC. The thermal efficiency η_2 can be written as

$$\eta_2 = \frac{P_2}{q_{in}} = \frac{J_2 A_2 \left[\frac{RT_{in}}{F}\ln[1 + p_{sat}(T_{in})\mu D_2/(RT_{in})] - V_{ac,2} - V_{R,2}\right]}{J_1 A_1 ML/F + J_1 A_1 c_P (T_H - T_{in}) M/F + A_1 \sigma \left(T_H^4 - T_{in}{}^4\right)/z}, \quad (3)$$

where in this case [14,26]

$V_{R,2} = J_2 D_2 [1.62 \times 10^{-5} T_{in} \exp(-45.5/T_{in}) + 1.55 \times 10^{-7} T_{in} \exp(3722/T_{in})]$,

$$V_{ac,2}=-\frac{2RT_{in}}{F}\ln\left[\frac{1}{2}\left[\frac{{J_2}^2T_{in}}{{B_2}^2p_{sat}^2(T_{in})}+4\right]^{\frac{1}{2}}-\frac{1}{2}\frac{J_2\sqrt{T_{in}}}{B_2p_{sat}(T_{in})}\right]+$$

$$\frac{2RT_{in}}{F}\ln\left[\frac{1}{2}\left[\frac{{J_2}^2\sqrt{T_{in}T_C}}{{B_2}^2p_{sat}(T_{in})p_{sat}(T_C)}+4\left[1+\frac{\left(1+\frac{3G_2}{8\pi}\right)\sqrt{2\pi MRT_{in}T_C}\frac{J_2}{F}}{p_{sat}(T_C)\sqrt{T_{in}}}\right]\right]^{\frac{1}{2}}\right.$$

$$\left.+\frac{1}{2}\frac{J_2(T_{in}T_C)^{\frac{1}{4}}}{B_2\sqrt{p_{sat}(T_{in})p_{sat}(T_C)}}\right],$$

$V_{R,2}$ indicates the second stage ionic BASE voltage, $V_{ac,2}$ is the second stage over potential difference, G_2 means the second stage pressure loss geometric factor, J_2 indicates the second stage current density, and B_2 stands for the second stage charge-exchange coefficient. Similarly, some parameters including T_{in}, μ, D_2, and T_C should satisfy the following equation [26]

$$\frac{p_{sat}(T_{in})}{1+p_{sat}(T_{in})\mu D_2/(RT_{in})}=p_{sat}(T_C)\sqrt{\frac{T_{in}}{T_C}}. \tag{4}$$

$$J_1A_1c_P(T_H-T_{in})M/F+J_1A_1ML/F+A_1\sigma\left(T_H^4-{T_{in}}^4\right)/z=P_2+J_2A_2c_P(T_{in}-T_C)M/F+$$
$$J_2A_2ML/F+A_2\sigma\left(T_{in}^4-{T_C}^4\right)/z \tag{8}$$

2.3. The efficiency of the two-stage Na-TEC

From Eqs. (1) and (3), the thermal efficiency, η, of the two-stage system can be expressed as

$$\eta=\frac{P}{q_H}=\eta_1+\eta_2(1-\eta_1), \tag{5}$$

where the power output of the whole device is,

$$P=P_1+P_2=q_H-J_2A_2ML/F-J_2A_2c_P(T_{in}-T_C)M/F-A_2\sigma\left(T_{in}^4-{T_C}^4\right)/z$$
$$=J_1A_1\left[\frac{RT_H}{F}\ln[1+p_{sat}(T_H)\mu D_1/(RT_H)]-V_{ac,1}-V_{R,1}\right]+$$
$$J_2A_2\left[\frac{RT_{in}}{F}\ln[1+p_{sat}(T_{in})\mu D_2/(RT_{in})]-V_{ac,2}-V_{R,2}\right] \tag{6}$$

The particular cases addressed in sections 2.1 and 2.2 can be recovered from the above equations with the appropriate selection of parameters (see Appendix A).

Table 1
Parameters used in the two-stage Na-TEC [2,9,27].

T_H(K)	1300
B_1(A K$^{1/2}$/(P$_a$ m^2))	50
B_2(A K$^{1/2}$/(P$_a$ m^2))	600
F(C/mol)	96485
c_P(J/(g K))	1.285
μ(m^2)	10^7
L(J/g)	4480
M(g/mol)	23
G_1	10
G_2	10
σ(W/(m^2 K^4))	5.67×10^{-8}
Z	50
R(J/(mol K))	8.314

3. The MEF and MPOD of the two-stage system

Eqs. (5) and (6) indicate that both η and P of the two-stage system depend on several crucial parameters including T_H, T_{in}, T_C, J_1, J_2, A_1, A_2, D_1, and D_2 (some other parameters not involved in the optimization have been fixed to typical values for this analysis, see Table 1). The last four of them involve an optimization on the design since they are related to the BASE geometry. It is convenient to introduce the power output density (POD), i.e., $p=P/A_1$, so that the area ratio A_1/A_2 may be taken as a parameter. T_H can be fixed to the maximum attainable value, which is also listed in Table 1. The remainder can be considered as operation variables. Among these variables, besides the constraint conditions given by Eqs. (2) and (4), there also exist two constraint relations imposed by the current continuity and energy conservation as follows

$$J_1A_1=J_2A_2 \tag{7}$$

and

According to the analyses above, there are only three independent variables for the two-stage Na-TEC shown in Fig. 1. For example, we can choose T_{in}, D_2, and J_1 as independent variables to optimize the performance of the two-stage Na-TEC. When T_{in} is a given value, Eqs. (5) and (6) and the parameter values given in Table 1 can be used to generate the 3D-graphs of the efficiency η and POD p varying with J_1 and D_2, as displayed in Fig. 2(a) and (b), respectively. It is observed from Fig. 2 that there exist the different optimal values of J_1 and D_2 to maximize η and p. When D_2 is optimally chosen, the influences of J_1 on both η and p are shown in Fig. 3(a), where $\eta_{\max,T_{in}}$ and $p_{\max,T_{in}}$ are the local MEF and MPOD of the two-stage Na-TEC for a given T_{in}, $p_{\eta_{\max},T_{in}}$ and $\eta_{p_{\max},T_{in}}$ are the POD at the local MEF and the efficiency at the local MPOD, respectively, and $J_{1,\eta_{\max},T_{in}}$ and $J_{1,p_{\max},T_{in}}$ are the optimal values of J_1 at the local MEF and MPOD. Fig. 3(a) displays that there are a local MEF $\eta_{\max,T_{in}}\approx36.2\%$ increasing about 34.1% and 24.8% compared with that of the two-stage Na-TECs mentioned in Refs. [9,23], respectively, and a local MPOD $p_{\max,T_{in}}\approx40.6\times10^3$ W/m^2. The $\eta\tilde{}p$ characteristic curve depicted in Fig. 3(b) shows more clearly the optimally operating region of the two-stage Na-TEC. In the ranges of $p<p_{\eta_{\max},T_{in}}$ and $\eta<\eta_{p_{\max},T_{in}}$, p increases with the increase of η. Thus, the system should be operated in the ranges of

$$\eta_{p_{\max},T_{in}}\le\eta\le\eta_{\max,T_{in}} \tag{9}$$

and

$$p_{\eta_{\max},T_{in}}\le p\le p_{\max,T_{in}}. \tag{10}$$

The optimal range of J_1 can be also determined by

$$J_{1,\eta_{\max},T_{in}}\le J_1\le J_{1,p_{\max},T_{in}}, \tag{11}$$

as it can be seen from Fig. 3(a).

4. Effects of T_{in}

In the above section, the intermediate temperature T_{in} was taken as a constant. However, this temperature plays a fundamental role in the overall performance of the two-stage Na-TEC. Below, we will analyse in detail the influences of T_{in} on the optimized regimes of the efficiency and

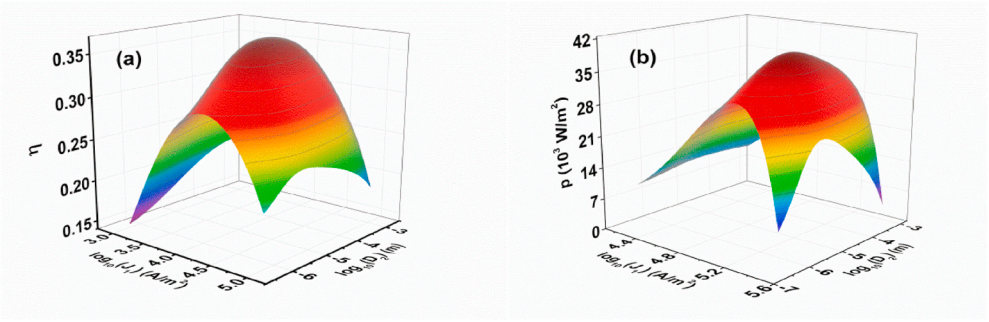

Fig. 2. (a) η and (b) p as functions of J_1 and D_2 at $T_{in} = 800$ K.

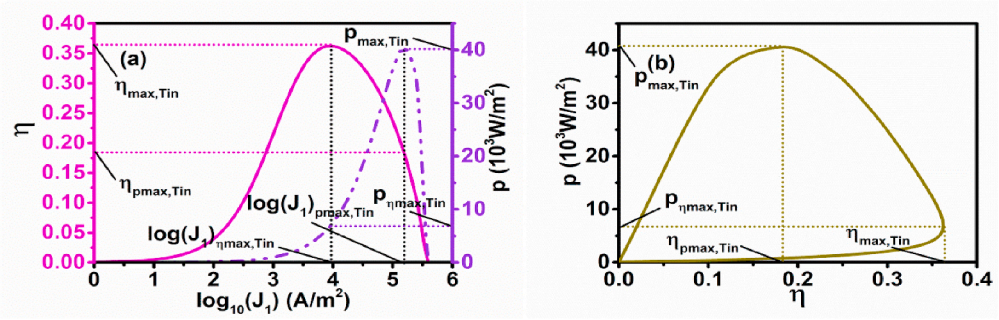

Fig. 3. (a) η and p as functions of J_1 and (b) the curve of p versus η at $T_{in} = 800$ K, where D_2 has been optimized.

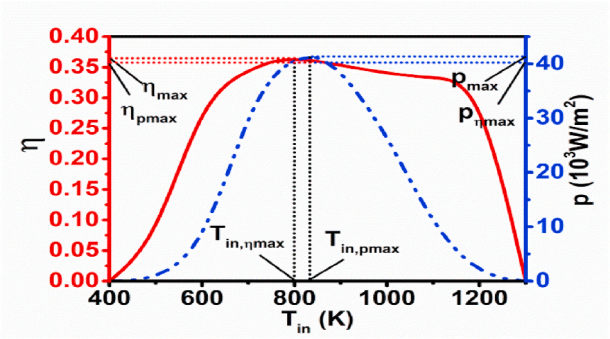

Fig. 4. η and p as functions of T_{in}, where J_1 and D_2 are such that it optimizes efficiency and POD.

POD.

Eqs. (5) and (6) can be further used to discuss the effects of T_{in} on both $\eta_{\max,T_{in}}$ and $p_{\max,T_{in}}$, as shown in Fig. 4, where J_1 and D_2 have been optimized, $\eta_{p_{\max}}$ and $p_{\eta_{\max}}$ are the optimal values of η at the MPOD and p at the MEF, and $T_{in,\eta}$ and $T_{in,p}$ are the optimal values of T_{in} at the MEF and MPOD. When $T_{in} = 800K \equiv T_{in,\eta}$, the system attains its MEF, i.e., $\eta_{\max} = 36.2\%$. When $T_{in} = 840K \equiv T_{in,p}$, the system attains its MPOD, i.e., $p_{\max} = 41.2 \times 10^3$ W/m^2. The optimal region of T_{in} can be determined by

$$T_{in,\eta_{\max}} \le T_{in} \le T_{in,p_{\max}}, \tag{12}$$

and the optimal regions of η and p are then re-expressed as

$$\eta_{p_{\max}} \le \eta \le \eta_{\max}, \tag{13}$$

$$p_{\eta_{\max}} \le p \le p_{\max}. \tag{14}$$

It is noteworthy that both the efficiency and the POD are capable of achieving considerable values when T_{in} satisfies Eq. (12). The optimal range of T_{in} isn't large and special attention should be paid to this problem in the design of two-stage Na-TECs.

When the two-stage Na-TEC is operated at the optimal states, which are in the ranges satisfied by Eqs. (13) and (14), the optimum values of T_C, A_1/A_2, J_1, J_2, D_1, and D_2, which are represented by $T_{C,\eta_{\max}}$ and $T_{C,p_{\max}}$, $(A_1/A_2)_{\eta_{\max}}$ and $(A_1/A_2)_{p_{\max}}$, $J_{1,\eta_{\max}}$ and $J_{1,p_{\max}}$, $J_{2,\eta_{\max}}$ and $J_{2,p_{\max}}$, $D_{1,\eta_{\max}}$ and $D_{1,p_{\max}}$, $D_{2,\eta_{\max}}$ and $D_{2,p_{\max}}$, are closely dependent on T_{in}, as shown in Fig. 5. $T_{C,\eta_{\max}}$, $(A_1/A_2)_{\eta_{\max}}$, $J_{1,\eta_{\max}}$, $J_{2,\eta_{\max}}$, and $D_{2,\eta_{\max}}$ are obviously different from $T_{C,p_{\max}}$, $(A_1/A_2)_{p_{\max}}$, $J_{1,p_{\max}}$, $J_{2,p_{\max}}$, and $D_{2,p_{\max}}$. The shaded regions between the red lines and the blue dash dot dots are the optimized regions of T_C, A_1/A_2, J_1, J_2, and D_2, which are determined by.

$$T_{C,\eta_{\max}} \le T_C \le T_{C,p_{\max}}, \tag{15}$$

$$(A_1/A_2)_{p_{\max}} \le A_1 \Big/ A_2 \le (A_1/A_2)_{\eta_{\max}}, \tag{16}$$

$$J_{1,\eta_{\max}} \le J_1 \le J_{1,p_{\max}}, \tag{17}$$

$$J_{2,\eta_{\max}} \le J_1 \le J_{2,p_{\max}}, \tag{18}$$

and

$$D_{2,p_{\max}} \le D_2 \le D_{2,\eta_{\max}}, \tag{19}$$

as shown in Fig. 5(a–d) and (f), respectively. It is clearly seen from Eq. (2) that D_1 depends only on T_{in} and T_H. For the given values of T_{in} and T_H, D_1 is a determinate quantity, which is independent of the state of the MEF or MPOD, so that $D_{1,\eta_{\max}}$ and $D_{1,p_{\max}}$ are the same, as indicated in Fig. 5(e).

5. Results and comparison with previous works

When $T_{in} = T_H$ or $T_{in} = T_C$, one can obtain the expressions of the efficiency η and power output P of a single Na-TEC (see Appendix A), i.e. [18]

and

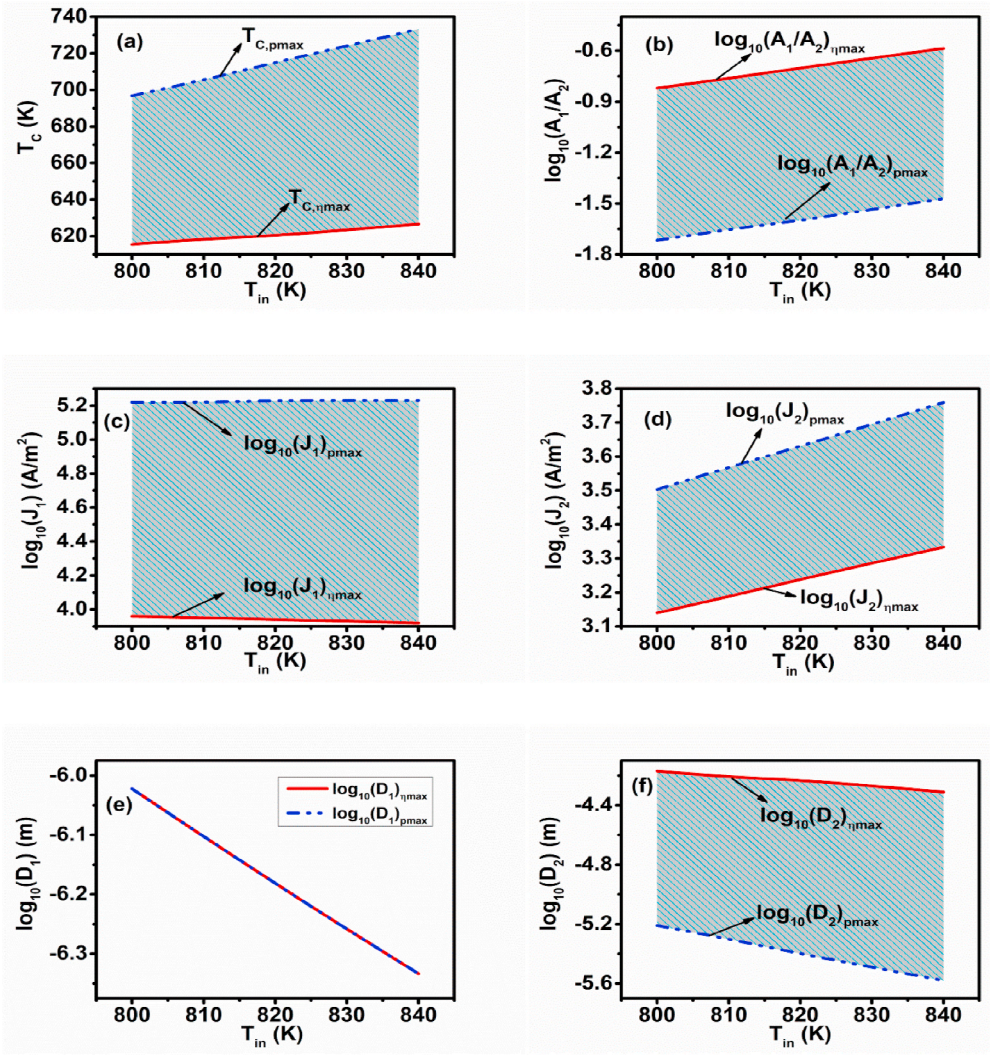

Fig. 5. (a) T_C, (b) A_1/A_2, (c) J_1, (d) J_2, (e) D_1 and (f) D_2 as functions of T_{in}.

$$P = JA\left[\frac{RT_H}{F}\ln[1 + p_{sat}(T_H)\mu D/(RT_H)] - V_{ac} - V_R\right], \tag{21}$$

$$\eta = \frac{J\left[\frac{RT_H}{F}\ln[1 + p_{sat}(T_H)\mu D/(RT_H)] - V_{ac} - V_R\right]}{J\left[\frac{RT_H}{F}\ln[1 + p_{sat}(T_H)\mu D/(RT_H)] - V_{ac} - V_R\right] + JML\Big/F + Jc_P(T_H - T_C)M\Big/F + \sigma\left(T_H^4 - T_C{}^4\right)\Big/z}, \tag{20}$$

By using Eqs. (5), (6), (20) and (21), we can plot the optimized curves of the efficiency versus the POD of a two-stage Na-TEC and a single Na-TEC operating at the same temperature span, as indicated by Fig. 6. As can be observed, the optimized performance of a two-stage Na-TEC is better than that of a single Na-TEC. The MEF and MPOD of a two-stage Na-TEC are 36.2% and 41.2×10^3 W/m^2, while the MEF and MPOD of a single Na-TEC are only 30.8% and 29.3×10^3 W/m^2 [18]. The MEF and MPOD of the former increase 17.5% and 40.6% compared with those of the latter. Besides, the MEF of the two-stage Na-TEC mentioned here increase 34.1% and 24.8% compared with the MEFs 27.0% and 29.0% of two-stage Na-TECs reported in Refs. [9,23]. This shows that the performance of two-stage Na-TECs can be largely improved through the optimum design. Two additional comments on the comparison of different results are in order at this point.

Firstly, the comparison between operation of the single- and dual-stage Na-TEC can be done mainly under two different conditions: at the same temperature of the external reservoirs, on one side, and a fixed heat input and a fixed hot-side temperature, on the other side. In the case of the same extreme temperatures a comparison is presented in Fig. 6 (inner curve) where it is appreciated clearly as the loop-like of density power versus efficiency is the same but in the single stage case both efficiency as power density have significant smaller values (29.3×10^3 W/m^2 and 30.8%) compared with those obtained in the two-stage case (41.2×10^3 W/m^2 and 36.2%). Under different temperatures ranges results may significantly differ. For instance, in Ref. [18] values for a single AMTEC with high temperature of 1170 K and the optimized values were found to be around 7000 W/m^2 and 23% for maximum power density and efficiency, respectively, although small variations

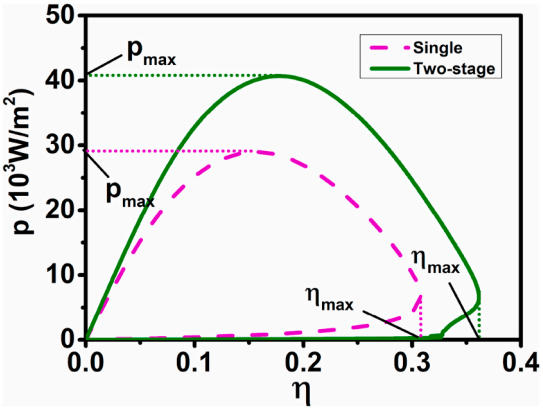

Fig. 6. The optimized curves of efficiency versus the POD for a two-stage Na-TEC and a single Na-TEC operating at the same temperature span.

can be produced depending on the remainder parameter being optimized (current density or thickness of BASE).

Secondly, it should be noted that a proper comparison of the values for power output and efficiency here presented with those of previous two-stage works [9,23] is not straightforward, both for the different theoretical point of view and for the mathematical methods. In Ref. [23] the reported maximum efficiency was 29% (with 4500 A/m^2 < J_1 < 5500 A/m^2) and a maximum power output of 125 W. In that case conduction bypass through the Na-TEC liquid-return path, corrugated geometries with radiation shields were considered by a mathematical finite-element model. In Refs. [9] the MEF reported is 27% at T_{in} around 775 K with $J_1 = 3500$ A/m^2 and $A_1/A_2 = 0.5$ while maximum power density is monotonically increasing with T_{in}, obtaining a value around 2000 W/m^2 at $T_{in} = 1050$ K. For that case, values $T_{evap} = 1150$ K and $T_{cond} = 550$ K were considered and the model was based on numerical simulations for the conduction heat transfer through the walls and the capillary wick of the device, plus radiative heat transfer from the cathode to the condenser, where the parasitic losses are proportional to the temperature dependence between the evaporator and the condenser. Here, POD and MEF states are achieved at intermediate temperatures T_{in} of 840 K and 800 K, respectively (see Fig. 4) allowing to establish upper and lower bounds for optimum values. In particular, the MEF is found at 800 K with J_1 around 10000 A/m^2 (see Fig. 5c) and A_1/A_2 value around 0.16 (see Fig. 5b), but now $T_H = 1300$ K and T_C is also an optimized parameter with values around 620 K (see Fig. 5a). The maximum POD is found around 40 kW/m^2 at $T_{in} = 840$ K and displaying values somewhat higher for J_1 and T_C but smaller for A_1/A_2. Notice that the definition of POD differs from the one considered by Limia et al. [9], defined as $P/(A_1 + A_2)$, meanwhile in the present case it is defined as P/A_1. Above considerations point out that the main difference between both approaches could be a consequence from the optimization scheme rather than from a structural design. For instance, in Ref. [9] a monotonous increasing power density (with respect to the intermediate temperature) is reported while the efficiency exhibits a parabolic-like behaviour with a well-defined maximum around 750 K. This feature differs from the present case (see Fig. 4) where a parabolic-like behaviour is displayed for both power density and efficiency. Thus, the parametrization of power versus efficiency (through elimination of T_{in}) produce the loop-like behaviour in Fig. 6, which sometimes is considered as a signature for the performance of real heat devices.

6. Multi-parametric and multi-objective optimization predictions

The parametric optimization of the single objective function like the efficiency or the POD of the two-stage Na-TEC has been obtained by using three independent variables J_1, T_{in}, and D_2 (directly linked to T_C). Herein, Pareto front [28–30] displays the best compromise among desirable quantities where a further improvement in one function involves the degrading of the rest, which is based on numerical multi-parametric and multi-objective optimization methods. The results obtained are shown in Fig. 6. A global optimization involving the simultaneous optimization of three independent parameters (J_1, T_{in}, and T_C) and two objective functions POD and efficiency could be realized. Reasonable values for J_1, T_{in}, and T_C are such that $800K \leq T_{in} \leq 1300K$, $400K \leq T_C \leq 800K$, and $\eta, \eta_1, \eta_2, P, P_1$, and P_2 are all positive quantities. Simultaneously, the multi-objective optimization is completed for the three configurations including the overall system, the first-stage Na-TEC, and the second-stage Na-TEC with the purpose of comparing the optimization of them. The physical variable space is displayed in Fig. 7(a). A random search in the physical region produces a first generation of points in the $\eta \tilde{} p$ space which are mapped into the energetic space depicted in Fig. 7(b) for the isolated second-stage Na-TEC, isolated first-stage Na-TEC, and the two-stage Na- TEC system.

It is worth noting that it is impossible to obtain an optimum configuration for POD and efficiency in the isolated second-stage system because of the limited range of J_1 . This is a straightforward consequence of the current continuity $J_1A_1 = J_2A_2$ joined to the cut-off current J_1 (see Fig. 3(a)). Both features impose constraints on J_2 which prevent the optimum configuration of the isolated second-stage system.

In the case of isolated configuration of the first-stage Na-TEC, there is a clear compromise region between the MPOD and the MEF operation regimes. Besides, the space of parameters in Fig. 7(a) indicates a preference for temperature $T_{in} \approx 800$ K which allows to obtain the MEF and MPOD for the first-stage Na-TEC; additionally, in a slender range for the T_{in} values it can be observed a noticeable improvement in both the efficiency and POD of the whole system, in agreement with the result exhibited in Fig. 4. It is indicated that the first-stage design should be modified with a small variation not to operate in its optimum configuration, leading to an obvious improvement of the overall system performance; raising the POD up to almost 41.4% and the MEF up to almost 29.1%, as shown in Fig. 7(b).

7. Conclusions and perspectives

A novel axisymmetric two-stage Na-TEC system including the main losses has been displayed. The matching problem between the first and second stages has been addressed with some outstanding results that can be beneficial for the development of high-performance duel-stage Na-TEC systems. Several significant results are listed:

(i)The specific impact of key parameters including the BASE area ratio of the first stage to the second stage, the intermediate plenum temperature, the thickness of the electrolyte of the second stage, and the current density of the first stage have been discussed. Accordingly, the optimum selective criteria of these parameters leading to optimized upper and lower bounds of the POD and efficiency have been identified and analysed. Special emphasis has been paid on the calculated the optimized parameters and the optimal intermediate temperatures. These last values define a quite narrow interval in between which the power output density and thermal efficiency of the overall device get their respective maximum values. This point could be of some importance from a design point of view.

(ii) The energetic performance of the duel-stage Na-TEC system is better than that of the single Na-TEC, as it can be checked in the loop-like behaviour of POD versus efficiency for both configurations. Herein, the MEF and MPOD of the duel-stage Na-TEC increase about 17.5% and 40.6% compared with those of the single Na-TEC. The energetic advantages of the present system are more obvious than those of other duel-stage systems. Specifically, the MEF of the two-stage Na-TEC increase 34.1% and 24.8% compared with those of two-stage Na-TECs reported in Refs. [9,

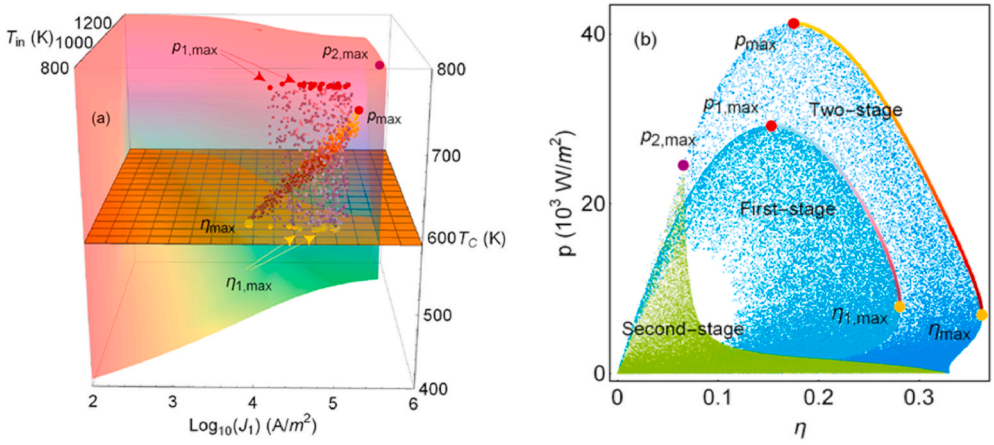

Fig. 7. (a) Parameter space bounded by the depicted surface indicating the region of physical interest. All possible physical configurations including the first-stage, the second-stage, and the whole system are depicted. (b) Pareto front is shown by energetic representation in the $\eta \tilde{} p$ space.

23]. Thus, a two-stage Na-TEC can be chosen for applications requiring high-performance.

(iii) The multi-parametric and multi-objective optimization analysis on the basis of the Pareto front and physically available space of states indicate that the configuration of optimum performance for the first stage system matches partially that for the two-stage system; this feature is endorsed by previous results. The differences between the optimum behaviors for collective and individual systems could be explained on the basis of linear irreversible thermodynamics [24,25] framework. See detail below.

The study displayed here is subject to a further extension to take into account various heat and fuel sources such as the external combustion, the nuclear reactor, the waste heat, or concentrated solar, in order to guide the design of more efficient and sustainable Na-TECs. Finally, it should be mentioned that the perspective of designing multi-step TEC beyond the two-stage model were presented [9,22]. At least theoretically, there exists linear irreversible thermodynamics models for arrays of coupled heat engines working between arbitrary temperature differences. A characteristic feature of these models is a control parameter which may select different operation regimes for the whole array without imposing the same operation regime to every engine in the array [24,25]. In other words, the selected intermediate temperatures could affect the more efficient operation regime in each case for both the collective and individual behaviours. Another notable feature is that these models are amenable to describe the corresponding refrigeration systems [25]. All together open novel perspectives to analyse multi-step TEC energy systems where the bridge between the individual and collective behaviours depends on specific set of transport coefficients and the temperature profile, thus allowing a unified thermodynamic description of TECs.

CRediT authorship contribution statement

Wanli Peng: Conceptualization, Methodology, Software, Formal analysis, Writing - original draft, Writing - review & editing. **Julian Gonzalez-Ayala:** Software, Formal analysis, Writing - review & editing. **Shanhe Su:** Validation, Formal analysis, Visualization. **Jincan Chen:** Resources, Conceptualization, Writing - review & editing, Supervision, Data curation. **Antonio Calvo Hernández:** Resources, Conceptualization, Writing - review & editing, Supervision, Data curation.

Declaration of competing interest

The authors declare that they have no known competing financial interests or personal relationships that could have appeared to influence the work reported in this paper.

Acknowledgments

This work has been supported by China Scholarship Council under the State Scholarship Fund (No. 201906310095). J. G. A. acknowledges Instituto Universitario de Física Fundamental y Matemáticas. We thank the Reviewers for their valuable suggestions.

Appendix A

When $T_{in} = T_H$, one can delete constraint equations (7) and (8) and get $J_1 = 0$, $D_1 = 0$, $\eta_1 = 0$, and $p_1 = 0$, i.e., the first-stage is disappeared. Eqs. (5) and (6) can be written as

$$\eta = \eta_2 = \frac{J_2\left[\frac{RT_H}{F}\ln[1 + p_{sat}(T_H)\mu D_2/(RT_H)] - V_{ac,2} - V_{R,2}\right]}{J_2\left[\frac{RT_H}{F}\ln[1 + p_{sat}(T_H)\mu D_2/(RT_H)] - V_{ac,2} - V_{R,2}\right] + J_2 ML \Big/ F + J_2 c_P (T_H - T_C) M \Big/ F + \sigma\left(T_H^4 - T_C^4\right) \Big/ z} \tag{A1}$$

and

$$P = P_2 = J_2 A_2 \left[\frac{RT_H}{F}\ln[1 + p_{sat}(T_H)\mu D_2/(RT_H)] - V_{ac,2} - V_{R,2}\right] \tag{A2}$$

When $T_{in} = T_C$, one can delete constraint equations (7) and (8) and get $J_2 = 0$, $D_2 = 0$, $\eta_2 = 0$, and $p_2 = 0$, i.e., there does not exist the second-stage. Eqs. (5) and (6) can be written as

$$\eta = \eta_1 = \frac{J_1\left[\frac{RT_H}{F}\ln[1+p_{sat}(T_H)\mu D_1/(RT_H)] - V_{ac,1} - V_{R,1}\right]}{J_1\left[\frac{RT_H}{F}\ln[1+p_{sat}(T_H)\mu D_1/(RT_H)] - V_{ac,1} - V_{R,1}\right] + J_1 ML \Big/ F + J_1 c_P (T_H - T_C) M \Big/ F + \sigma\left(T_H^4 - T_C^4\right) \Big/ z} \tag{A3}$$

and

$$P = P_1 = J_1 A_1 \left[\frac{RT_H}{F}\ln[1+p_{sat}(T_H)\mu D_1/(RT_H)] - V_{ac,1} - V_{R,1}\right] \tag{A4}$$

Obviously, Eqs. (A1)and (A2) exactly equal Eqs. (A3) and (A4), which represent the efficiency and power output of a single Na-TEC. For the sake of simplicity, subscript 2 in Eqs. (A1) and (A2) or subscript 1 in Eqs. (A3) and (A4) may be deleted so that Eqs. (20) and (21) are directly obtained from the above equations.

References

[1] Q. Wang, W. Yao, H. Zhang, X. Lu, Analysis of the performance of an alkali metal thermoelectric converter (AMTEC) based on a lumped thermal-electrochemical model, Appl. Energy 216 (2018) 195–211.

[2] T. Cole, Thermoelectric energy conversion with solid electrolytes, Science 221 (1983) 915–920.

[3] J.M. Merrill, C. Mayberry, Experimental investigation of multi-AMTEC cell ground demonstration converter systems based on PX-3 and PX-5 series AMTEC cells, AIP Conf. Proc. 458 (1999) 1369–1377.

[4] N. Weber, A thermoelectric device based on beta-alumina solid electrolyte, Energy Convers. 14 (1974) 1–8.

[5] R.M. Williams, M.E. Loveland, B. Jeffries-Nakamura, M.L. Underwood, C. P. Bankston, H. Leduc, J.T. Kummer, Kinetics and transport at AMTEC electrodes: I. The interfacial impedance model, J. Electrochem. Soc. 137 (1990) 1709–1716.

[6] R.M. Williams, B. Jeffries-Nakamura, M.L. Underwood, C.P. Bankston, J. T. Kummer, Kinetics and transport at AMTEC electrodes: II. Temperature dependence of the interfacial impedance of Na (g)/Porous Mo/Na-beta′ alumina, J. Electrochem. Soc. 137 (1990) 1716–1723.

[7] M.T. Dunham, B.D. Iverson, High-efficiency thermodynamic power cycles for concentrated solar power systems, Renew. Sustain. Energy Rev. 30 (2014) 758–770.

[8] A. Gunawan, A. Limia, J.M. Ha, P.A. Kottke, S.W. Lee, A.G. Fedorov, S.K. Yee, Techno-economic analysis of dual-stage sodium thermal electrochemical converter (Na-TEC) power block for distributed CSP, Proc. ASME Int. Conf. Energy Sustain. Paper No: ES2018-7505, V001T11A008; https://doi.org/10.1115/ES2018-7505.

[9] A. Limia, J.M. Ha, P. Kottke, A. Gunawan, A.G. Fedorov, S.W. Lee, S.K. Yee, A two-stage sodium thermal electrochemical converter (Na-TEC), J. Power Sources 371 (2017) 217–224.

[10] J.M. Tournier, M.S. El-Genk, Performance analysis of Pluto/Express, multitube AMTEC cells, Energy Convers. Manag. 40 (1999) 139–173.

[11] S.P.S. Badwal, S.S. Giddey, C. Munnings, A.I. Bhatt, A. F Hollenkamp, Emerging electrochemical energy conversion and storage technologies, Front. Chem. 2 (2014) 79.

[12] H. Nakata, T. Nagata, K. Tsuchida, A. Kato, Ceramic electrodes for an alkali metal thermo-electric converter (AMTEC), J. Appl. Electrochem. 23 (1993) 1251–1258.

[13] M.A.K. Lodhi, A. Daloglu, Effect of geometrical variations on AMTEC cell heat losses, J. Power Sources 91 (2000) 99–106.

[14] M.A.K. Lodhi, P. Vijayaraghavan, A. Daloglu, An overview of advanced space/terrestrial power generation device: AMTEC, J. Power Sources 103 (2001) 25–33.

[15] M.A.K. Lodhi, S.C. Soon, M. Mohibullah, Temperature-dependent grain growth model for AMTEC electrodes, J. Power Sources 135 (2004) 304–310.

[16] M.A.K. Lodhi, P. Vijayaraghavan, A. Daloglu, Time-dependent BASE performance and power degradation in AMTEC, J. Power Sources 93 (2001) 41–49.

[17] M. El Genk, J.M. Tournier, Recent advances in vapor-anode, multi-tube, alkali metal thermal-to-electric conversion cells for space power, Proc. Fifth Eur. Space Power Conf. 416 (1998) 257.

[18] W. Peng, X. Zhang, Z. Ye, J. Chen, Optimum operation states and parametric selection criteria of an updated alkali metal thermal electric converter, Energy Convers. Manag. 168 (2018) 230–236.

[19] S.Y. Wu, Y.C. Zhang, H. Yang, L. Xiao, Performance evaluation and parametric analysis of AMTEC/TEG hybrid system, Energy Convers. Manag. 154 (2017) 118–126.

[20] W. Peng, W. Li, Z. Ye, G. Su, J. Chen, Parametric design strategies of an updated alkali metal thermoelectric converter-thermoelectric generator system operating at optimum states, Energy Convers. Manag. 182 (2019) 53–59.

[21] W. Peng, J. Gonzalez-Ayala, J. Guo, J. Chen, A.C. Hernández, An alkali metal thermoelectric converter hybridized with a Brayton heat engine: parametric design strategies and energetic optimization, J. Clean. Prod. 120953 (2020).

[22] S. Balagopal, A.V. Joshi, S. John, Multi-stage sodium heat engine for electricity and heat production, U.S. Patent Appl. No. 15/273,367.

[23] A. Limia, P. Kottke, A.G. Fedorov, S.K. Yee, Thermal modeling and efficiency of a two-stage sodium heat engine, Appl. Therm. Eng. 145 (2018) 603–609.

[24] B.J. De Cisneros, A.C. Hernández, Collective working regimes for coupled heat engines, Phys. Rev. Lett. 98 (2007) 130602.

[25] B.J. De Cisneros, A.C. Hernández, Coupled heat devices in linear irreversible thermodynamics, Phys. Rev. E 77 (2008), 041127.

[26] S.Y. Wu, L. Xiao, Y. Cao, Y.R. Li, A parabolic dish/AMTEC solar thermal power system and its performance evaluation, Appl. Energy 87 (2010) 452–462.

[27] J.M. Tournier, M.S. El-Genk, M. Schuller, P. Hausgen, An analytical model for liquid-anode and vapor-anode AMTEC converters, AIP Conf. Proc. 387 (1997) 1543–1552.

[28] K. Deb, Multi-objective Optimization Using Evolutionary Algorithms, vol. 16, John Wiley & Sons, 2001, 978-0-471-87339-6.

[29] C.A. Spence, M. Schuller, T.R. Lalk, Development, evaluation, and design applications of an AMTEC converter model, AIP Conf. Proc. 654 (2003) 685–700.

[30] J.M. Tournier, M.S. El-Genk, An electric model of a vapour anode, multitube alkali–metal thermal-to-electric converter, J. Appl. Electrochem. 29 (1999) 1263–1275.